HOKKAIDO UNIVERSITY

Title	Re-Estimating a Source Model for the 1923 Kanto Earthquake by Joint Inversion of Tsunami Waveforms and Coseismic Deformation Data
Author(s)	Nakadai, Yumi; Tanioka, Yuichiro; Yamanaka, Yusuke et al.
Citation	Bulletin of the Seismological Society of America, 113(5), 1856-1866 https://doi.org/10.1785/0120230050
Issue Date	2023-10
Doc URL	https://hdl.handle.net/2115/93357
Type	journal article
File Information	BSSA-D-23-00050_R2 (1).pdf

Hokkaido University Collection of Scholarly and Academic Papers : HUSCAP

Re-estimating a source model for the 1923 Kanto earthquake by joint inversion of tsunami waveforms and co-seismic deformation data

Yumi Nakadai[1)], Yuichiro Tanioka[2)], Yusuke Yamanaka[2)], and Tatsuya Nakagaki[3)]

1) NTT DATA Corporation, Toyosu Center Building, 3-3-3 Toyosu, Koto City, Tokyo, Japan, 135-0061
2) Institute of the Seismology and Volcanology, Faculty of Science, Hokkaido University, N10W8 Kita-ku Sapporo, Japan, 060-0810
3) Graduate School of Science, Hokkaido University, Sapporo, N10W8 Kita-ku Sapporo, Japan, 060-0810

Corresponding Author: Yuichiro Tanioka e-mail: tanioka@sci.hokudai.ac.jp

Abstract

The 1923 Kanto earthquake generated not only strong motions that caused a devastating disaster around the metropolitan Tokyo area but also a large tsunami. Although the slip distribution of the 1923 Kanto earthquake has been estimated by several researchers, tsunami waveforms observed at tide gauges near the source have never been used. In this study, the slip distribution of the 1923 Kanto earthquake was estimated using joint inversion of tsunami waveforms and vertical crustal deformations reported in historical documents. The estimated slip distribution was generally consistent with those estimated in previous studies except for a large slip of 9 m along the western portion of the plate interface, updip near the Sagami Trough. The east coast of the Izu Peninsula was inundated by the tsunami and surveyed after the tsunami to determine tsunami heights in the inundation areas. The

tsunami inundation computed from the estimated slip distribution explained the tsunami heights, and the large slip played an important role in large inundation. These results indicate that the large slip west of the Sagami Trough is essential for explaining the observed tsunami caused by the 1923 Kanto earthquake.

Key points

1) We estimate the source process of the 1923 Kanto earthquake by combining tsunami and vertical displacement data
2) Large slip (> 9 meters) near the western Sagami Trough is necessary to explain the tsunami observations
3) If available, tsunami data are important to constrain source processes of historical earthquakes

1. Introduction

The 1923 Great Kanto earthquake (Mw8.0) occurred at the interface of the Philippine Sea Plate, subducting along the Sagami Trough beneath the Tokyo metropolitan area (Figure 1a). The earthquake was one of the most devastating disasters in history, with more than 100,000 fatalities in the Tokyo metropolitan area. A large number of fires occurred in populated areas after the strong motion of the earthquake and caused a large number of fatalities (Imperial Earthquake Investigation Committee, 1925). The earthquake also generated a large tsunami, which caused damage along the coast of the Izu Peninsula (Aida, 1993).

The source processes of the 1923 Kanto earthquake were previously investigated using seismological and geodetical data. Kanamori (1971) determined the focal mechanism of the earthquake using P-wave polarity data and the seismic moment to be 7.6×10^{20} Nm (Mw 7.9) using surface wave amplitude data. Matsu'ura et al. (1980) and Matsu'ura and Iwasaki (1983) estimated the fault parameters using the geodetic data. Their fault models are consistent with the focal mechanism estimated by Kanamori (1971). Nyst et al. (2006) also analyzed the geodetic data to estimate the

improved two fault model. The geodetic and teleseismic data were simultaneously inverted to estimate the slip distribution by Wald and Somerville (1995). Their solution shows two large slip areas, one near the hypocenter and another at the southeast of the first one. Kobayashi and Koketsu (2005) estimated the source process of the earthquake by using a joint inversion of the geodetic, teleseismic and strong motion data. Their estimated slip distributions are similar to that estimated by Wald and Somerville (1995). Matsuura et al. (2007) estimated the slip distribution of the earthquake along the plate interface by the inversion of the geodetic data based on a Bayesian formulation. Their result also shows two large slip areas similar to those of Kobayashi and Koketsu (2005) and Wald and Somerville (1995). Aida (1993) indicated that large tsunami heights along the east coast of the Izu peninsula (Figure 1b), such as the height of 8-9m at Manazuru, cannot be explained by slip along the plate interface of the Philippine Sea Plate subducted along the Sagami Trough. He concluded that an additional high angle fault off the Izu Peninsula was necessary to explain those tsunami heights.

Tsunami waveforms were also observed at four tide gauges in Tokyo Bay and several tide gauges along the Pacific coast of Japan (Imperial Earthquake Investigation Committee, 1925). Therefore, it is important to determine whether the observed tsunami waveforms, particularly those observed near the source area, can be explained by the source models that were determined using geodetic and seismic data. In addition, it is important to determine a source model that can explain both those tsunami waveforms and large tsunami heights along the east coast of the Izu Peninsula.

In this study, joint inversion of geodetic data and tsunami waveforms was performed to estimate the slip distribution of the 1923 Kanto earthquake. The estimated slip distribution was compared with those estimated in previous studies (e.g., Koketsu and Kobayashi, 2005; Matsuura et al., 2007) to discuss the tsunami excitation caused by the earthquake. Tsunami heights along the east coast of the Izu Peninsula were also computed from the estimated slip distribution and compared with the large tsunami heights surveyed in this area to discuss the necessity of an additional fault off the Izu Peninsula

as suggested by Aida (1993).

2. Data

2.1 Crustal deformation data

The vertical co-seismic crustal deformation associated with the 1923 Kanto earthquake was measured by leveling surveys conducted in 1898 and 1923 before and after the earthquake, respectively, as reported by the Military Land Survey (1930), the predecessor of the Geospatial Information Authority of Japan. Those data were used in previous studies to estimate the slip distribution of the earthquake (e.g., Matsuura and Iwasaki, 1983; Koketsu and Kobayashi, 2005; Matsuura et al., 2007). Co-seismic vertical deformation data at 683 locations obtained from Namagaya et al. (2011) were used in this study (Figure 2).

2.2 Observed tsunami waveforms

The tsunami generated by the 1923 Kanto earthquake was recorded by several tide gauges along the Pacific coast of Japan and reported by the Imperial Earthquake Investigation Committee (1925). We selected four tsunami waveforms observed at tide gauges near the source area, Fukagawa, Shibaura, and Chiba in Tokyo Bay, and at Minato-machi in northern Kanto on the Pacific coast (Figure 1). The observed tsunamis arrived at the tide gauges at low tide. Those waveforms are sensitive to the slip distribution of the source beneath the Tokyo metropolitan area. First, these data were digitized using Simple Digitizer, software that reads numerical data from images. Next, similar to Yamanaka and Tanioka (2021), the heights of the astronomical tide for 720 minutes from the origin time of the earthquake were calculated at tide gauge stations using the short-period ocean tide model (NAO99Jb) of the ocean tide system NAOTIDEJ (Matsumoto et al., 2001). Tsunami waveform data were constructed by subtracting the calculated tidal heights from the original digitized data. The sampling

interval was set to 1 min. Tsunami waveforms with 120 min of data from the origin time of the earthquake were used to estimate earthquake slip distribution.

2.3 Bathymetry data

General Bathymetric Charts of the Oceans (GEBCO) 30-second grid data (Weatherall et al., 2015) are used to produce bathymetry data for our tsunami simulation in general. The Japan Hydrographic Association's bathymetric data M7001 was used around Tokyo Bay to resolve the bay bathymetry and geometry. However, since the 1923 Taisho Kanto Earthquake, the coastal landforms in Tokyo Bay have changed drastically because of reclaimed land development. Therefore, referring to an old map of the Taisho era (KTGIS.net), we modified the seafloor bathymetry data and removed the reclaimed land. Figure 3 compares the old map, a recent map, and an aerial photograph of recent Tokyo Bay area.

3. Method of Joint inversion

3.1 Fault Parameters and vertical deformations

As shown in Figure 4, 28 subfaults were distributed along the upper surface of the Philippine Sea Plate which was previously determined by Iwasaki et al. (2015) using various data including seismic refraction profiling, tomography, and seismic source distribution data. A rectangular subfault system cannot describe the upper surface of the Philippine Sea plate in this area because the dip angles of the plate interface along the source area of the 1923 Kanto earthquake changed rapidly from west to east (Figure 4). In this study, each subfault was divided into two triangular faults, as illustrated in Figure 4.

The vertical surface deformation caused by the fault motion of each subfault was calculated by adding the two surface deformations computed from the two triangular faults using algorithms for triangular dislocation elements in a uniform elastic half-space (Meade, 2007). The dip angles, strikes and depths

123 of the subfaults were calculated to fit the upper surface of the Philippine Sea Plate (Table 1 and
124 Supplemental Material). The slip direction was calculated to fit the directions of the slip deficit rate
125 from 1996 to 2000, as Sagiya (2004) estimated.
126
127 **3.2 Tsunami numerical simulation**
128 Synthetic waveforms (Green's functions) at the four stations from all subfaults in Figure 4 were
129 numerically computed by solving linear shallow water equations with a spherical coordinate system
130 (Goto, 1991). The grid spacing is set to 30 arc-sec. As the amplitudes of the observed tsunamis at the
131 four stations were less than 1m (Figure 5b), the effect of the nonlinearity was negligible. These
132 equations have been widely used in the tsunami waveform inversion studies (e.g., Gusman et al., 2012,
133 Fuji et al.,2011). The initial surface deformation of the tsunami was set as the vertical deformation in
134 the ocean bottom computed using the algorithms for triangular dislocation elements in a uniform
135 elastic half-space (Meade, 2007) for each subfault, as described in the previous section.
136
137 **3.2 Joint Inversion of tsunami waveforms and crustal deformation**
138 The slip distribution of the 1923 Kanto earthquake was estimated by joint inversion using tsunami
139 waveforms and vertical crustal deformation data. As previously explained, the dataset for the joint
140 inversion consisted of Green's functions for 120 min at four tide gauge stations and computed the
141 vertical deformation at 683 locations from 28 subfaults with the observations. A non-negative least
142 square method (Lawson and Hansonm 1974) was used for inversion. The joint inversion method has
143 been described by Satake (1993). A weighting factor (λ), a ratio of the relative power of two datasets,
144 must be defined. Based on the Euclidean norm ratio of the tsunami data and the crustal deformation
145 data, the weight of the crustal deformation data against the tsunami data (λ) was 0.538.
146 A "delete-half" Jackknife resample data set is generated from the original data by randomly deleting

147 half of the data points from each data set. The standard error of the slip distribution is calculated from
148 estimated slip distributions using 1000 “delete-half” Jackknife resample data sets (Tichelarr and Ruff,
149 1989).
150
151 **4. Method of Tsunami inundation simulation**
152 Using the slip distribution model estimated from the joint inversion, a tsunami inundation
153 simulation was conducted for an area near the source (Figure 1a). Tsunami inundation along the east
154 coast of the Izu Peninsula was numerically computed by solving non-linear shallow water equations
155 using the moving boundary condition. (e.g., Goto et al., 1997; Yanamaka and Tanioka, 2022). The
156 nonlinear shallow water equations include advection terms and bottom friction terms. The Manning’s
157 roughness coefficient is used in the bottom friction terms as a friction parameter. Homogeneous
158 Manning’s roughness coefficient of $0.025\ m^{-1/3}s$ is assumed, a value widely used in tsunami
159 inundation modeling (Imamura, 2009). The bathymetry and topography girds with a 2 arc-sec
160 resolution (i.e., approximately 50 ~ 60 m resolution) were first produced from the digital elevation
161 model (Geospatial Information Authority of Japan) and the M7001 digital bathymetric chart (the Japan
162 Hydrographic Association). The data near the survey locations in Aida (1993) were then modified by
163 referring to an old map from the Taisho era.
164
165 **5. Results**
166 **5.1 Results of joint inversion**
167 Figure 5a and Table 1 show the slip distribution estimated by joint inversion of the tsunami
168 waveforms and vertical crustal deformation data. Figure 5b compares the observed and computed
169 tsunami waveforms. Figure 6 compares the observed and computed vertical crustal deformations. Both
170 observed tsunami waveforms and vertical crustal deformations are well explained by the computed

ones. Two large slip areas were estimated: one near the epicenter of the earthquake, dashed ellipsoid I in Figure 5a, and the other at the plate interface beneath the Miura and Boso peninsulas, dashed ellipsoid II in Figure 5a. The seismic moment, Mw, calculated from the slip distribution in Table 1 is 1.49 x 10^{21} Nm (Mw 8.0) by assuming the rigidity of 3.0 x 10^{10} N/m^2. This result is similar to the previous studies (Kobayashi and Koketsu, 2005; Wald and Somerville, 1995; Matsuura et al., 2007). As an example, the slip distribution previously estimated by Matsuura et al. (2007) is shown in Figure 5a. However, the estimated slip distribution model indicated a large slip of 9 m at subfault 4C (Figure 5a) near the Sagami Trough, which has not been estimated in previous studies. Furthermore, to confirm how a large slip at the subfault 4C was necessary, we carried out the joint inversion with several different conditions so that the weight of the crustal deformation data against the tsunami data (λ) varied from 0.25 to 2.0. Figure 7 shows the slip distributions estimated using five different weights. The joint inversion with a larger weight of crustal deformation had a smaller slip amount on subfault 4C. This suggests that a large slip amount of subfault 4C was necessary to explain mainly the observed tsunami waveforms but not much of the observed crustal deformation data. This result is the same as the slip resolution along the Nankai Trough estimated by Sagiya and Thatcher (2006). They showed that slips at the plate interface near the trough is sensitive to the tsunami waveforms but not the geodetic data. We also computed tsunami waveforms from the estimated slip distribution without subfault 4C and compared those with the observed tsunami waveforms (APPENDIX). Variance reduction with tsunami waveforms computed from all subfaults was 86.4%, while that with tsunami waveforms computed from those without subfault 4C decreased to 78.8 %.

5.2 Results of the tsunami inundation simulation

As mentioned previously, Aida (1993) indicated that large tsunami heights along the east coast of the Izu Peninsula could not be explained by the slip along the plate interface of the Philippine Sea Plate

(Supplemental Material). Because the large slip estimated at subfault 4C, which was different from the previous results, was deduced to produce a large tsunami, we numerically computed the tsunami inundation along the coasts using the slip distribution estimated by the joint inversion. The computed maximum and the observed tsunami heights are compared in Figure 8. The computed tsunami heights explained by the observed tsunami heights (Aida, 1993) well. We also computed tsunamis using the slip distribution without the slip at subfault 4C. In this case, the computed tsunami heights were clearly underestimated to those observed (Figure 8 and Supplemental Material). To evaluate the fitting between the observed and computed tsunami heights, we calculated the geometric mean ratio of Aida (1978) number *K* be written as

$$\boldsymbol{logK = \frac{1}{N}\sum_{i=1}^{N} log\frac{O_i}{S_i}}$$

where O_i and S_i are observed and computed tsunami heights, respectively. For the computed tsunami heights from the estimated slip distribution, K was 1.15, indicated that the observed and computed tsunami heights are comparable. For those from the slip distribution without 4C, K was 2.24, indicated that the computed tsunami heights clearly underestimate the observed ones. This confirms that a large slip at the subfault 4C is necessary to explain the observed tsunami waveforms and tsunami heights along the eastern coast of the Izu Peninsula.

6. Discussion

The survey results after the 1923 Kanto earthquake (Imperial Earthquake Investigation Committee, 1925) indicated that Hatsushima Island (Figure 8) was co-seismically uplifted about 1.5-1.8 m. The computed vertical uplift at Hatsushima Island from the estimated slip distribution was only a few centimeters, much smaller than the surveyed uplift. Therefore, the observed uplift was not caused by a slip at the plate interface along the subduction zone as indicated in previous studies (Hatori, 1983, Aida, 1993). Sources such as a high angle fault near Hatsushima Island may have been necessary to

generate this uplift. It might be a slow slip or an aseismic slip along the fault after the 1923 Kanto earthquake.

The previous large earthquake in this area was the 1703 Genroku Kanto earthquake (Figure 1) which generated larger tsunamis along the Pacific coast of the Chiba Prefecture than the 1923 Kanto earthquake (Namegaya et al. 2011). The source area of the 1703 Genroku Kanto earthquake extends east of the source area of the 1923 Kanto earthquake (Namagaya et al. 2011; Yanagisawa and Goto, 2017). The observed tsunami heights along the east coast of the Izu Peninsula caused by the 1703 earthquake were 5-8 m (Aida, 1993), similar to those caused by the 1923 Kanto earthquake shown in Figure 1. This indicates that the eastern extension of the source did not affect the maximum tsunami heights along the east coast of the Izu Peninsula as Yanagisawa and Goto (2017) indicated. This may also support that the 1923 Kanto earthquake re-ruptured the source area beneath the Tokyo metropolitan area of the 1703 Genroku Kanto earthquake with similar slip amounts.

7. Conclusions

The slip distribution of the 1923 Kanto earthquake was estimated using the joint inversion of tsunami waveforms and vertical crustal deformations. This result is consistent with the previous results except for a large slip of 9 m at the subfault 4C near the west of the Sagami Trough. The tsunami inundation computed from the estimated slip distribution explains the large tsunami heights observed along the east coast of the Izu Peninsula. We conclude that a large slip near the west of the Sagami Trough is necessary to explain the tsunami caused by the 1923 Kanto earthquake.

Data and Resources

Old maps of the Taisho era (KTGIS.net) are available at http://ktgis.net/kjmapw/index.html (last accessed March 2023). Gridded bathymetry data (GEBCO) are available at

https://www.gebco.net/data_and_products/gridded_bathymetry_data/gebco_30_second_grid/. The Japan Hydrographic Association's bathymetric data, M7001, are available at https://www.jha.or.jp/shop/index.php?main_page=product_info_js2&products_id=1365.

Supplemental Material for this article includes parameters of the subfaults used in the joint inversion (Table S1), a summary of the 1923 Kanto earthquake in Aida (1993), and surveyed tsunami heights along the eastern coast of the Ize peninsula described by Aida (1993) with those computed maximum tsunami heights (Table S2). The digitized tide gauge data without the tides are available at https://www.sci.hokudai.ac.jp/isv/data/tanioka-data202306.

Declaration of Competing Interests

The authors acknowledge there are no conflicts of interest recorded.

Acknowledgments

We greatly thank Dr. Namegaya for providing co-seismic deformation data used in Namegaya et al. (2011). We also thank two anonymous reviewers and the editor for useful and important comments to improve our study. This study was supported by the Ministry of Education, Culture, Sports, Science and Technology (MEXT) of Japan, under its The Second Earthquake and Volcano Hazards Observation and Research Program (Earthquake and Volcano Hazard Reduction Research).

References

Aida, I. (1978). Reliability of a tsunami source model derived from fault parameters, J. Phys. Eart*h*, **26**, 57– 73.

Aida, I. (1993). Historical tsunamis and their numerical models which occurred in the north-western part of Sagami bay, J. Geography, 102, 427-436 (in Japaness).

Fujii, Y., K. Satake, S. Sakai, M. Shinohara, and T. Kanazawa (2011). Tsunami source of the 2011 off the Pacific coast of Tohoku Earthquake, Earth Planets Space, 63, 815–820.

Goto C. (1991). Numerical Simulation of the Trans-oceanic Propagation of Tsunami. rep, 30. Port and Harbour Research Institute, 4–19 (In Japanese).

Goto C, Y. Ogawa, N. Shuto, and F. Imamura (1997). Numerical method of tsunami simulation with the leap-frog scheme (IUGG/IOC Time Project). IOC Manual. United Nations Educational, Scientific and Cultural Organization, 35.

Gusman, A. R., Y. Tanioka, S. Sakai, and H. Tsushima (2012). Source model of the great 2011 Tohoku earthquake estimated from tsunami waveforms and crustal deformation data**,** Earth Planet. Sci. Lett. 341–344, 234-242.

Hatori, T. (1983). Tsunami behavior of the 1923 Kanto earthquake at Atami and Hatsushima Island in Sagam Bay, Bull. Earthq. Res. Inst., 59, 683-689 (in Japanese).

Imamura, F. (2009). Tsunami modeling: Calculating inundation and hazard maps, in *The Sea, Volume 15:* Tsunamis, edited by E. N. Bernard and A. R. Robinson, chap. 10, pp. 321– 332, Harvard Univ. Press, Cambridge, Mass.

Imperial Earthquake Investigation Committee (1925). Report of Imperial Investigation Committee, 100, A-C (in Japanese).

Iwasaki, T., H. Sato, M. Shinohara, T. Ishiyama, and A. Hashima (2015). Fundamental structure model of island arcs and subducted plates in and around Japan, 2015 Fall Meeting, AGU, San Francisco, T31B-2878.

Kanamori, H. (1971). Faulting of the Great Kanto Earthquake of 1923 as revealed by seismological data, Bull. Earthq. Res. Inst, 49, 13-18

Kobayashi, R., and K. Koketsu (2005). Source process of the 1923 Kanto earthquake inferred from historical geodetic, teleseismic, and strong motion data, Earth Planets Space, 57, 261–270

291 Lawson, C. L. and R. J. Hanson, (1974). Solving Least Squares Problems, Prentice-Hall, Inc.,
292 Englewood Cliffs, N.J., 340pp
293 Military Land Survey (1930). Re-survey of the Kwanto district after the great earthquake of 1923,
294 Bull. Imp. Earthquake Investigation Committee, 11, 1–6.
295 Matsumoto, K., T. Takanezawa, and M. Ooe (2000). Ocean tide models developed by assimilating
296 TOPEX/POSEIDON altimeter data into hydrodynamical model: a global model and a regional
297 model around Japan, J. Oceanography, 56, 567-581.
298 Matsu'ura, M., A. Noda, and Y. Fukahata (2007) Geodetic data inversion based on Bayesian
299 formulation with direct and indirect prior information, Geophys. J. Int., 171, 1342-1351.
300 Matsu’ura, M. and T. Iwasaki (1983). Study on coseismic and postseismic crustal movements
301 associated with the 1923 Kanto Earthquake, Tectonophysics, 97, 201–215.
302 Matsu’ura, M., T. Iwasaki, Y. Suzuki, and R. Sato. (1980). Statical and dynamical study on faulting
303 mechanism of the 1923 Kanto earthquake, J. Phys. Earth, 28, 119–143.
304 Meade, B. J. (2007). Algorithms for the calculation of exact displacements, strains, and stresses for
305 triangular dislocation elements in a uniform elastic half space, Computers & Geosciences, 33, 1064-
306 1075.
307 Military Land Survey (1930). Re-survey of the Kwanto district after the great earthquake of 1923,
308 Bull. Imp. Earthquake Investigation Committee, 11, 1–6.
309 Namegaya Y, K. Satake, M. Shishimura (2011). Fault models of the 1703 Genroku and 1923 Taisho
310 Kanto earthquakes inferred from coastal movements in the southern Kanto area, Annu Rep Act Fault
311 Paleoearthq. Res 11:107–120 (in Japanese)
312 Nyst, M., T. Nishimura, F. F. Pollitz, and W. Thatcher (2006). The 1923 Kanto earthquake reevaluated
313 using a newly augmented geodetic data set, Journal of Geophysical Research: Solid Earth 111,
314 B11306.

315 Sagiya, T., and W. Thatcher (1999). Coseismic slip resolution along a plate boundary megathrust: the
316 Nankai Trough, southwest Japan, J. Geophys. Res. 104 1111-1129.
317 Sagiya, T. (2004). Interplate Coupling in the Kanto District, Central Japan, and the Boso Peninsula
318 Silent Earthquake in May 1996, Pure and Appl. Geophys., 161, 2327–2342.
319 Satake, K. (1993). Depth distribution of coseismic slip along the Nankai Trough, Japan, from joint
320 inversion of geodetic and tsunami data, J. Geophys. Res.: Solid Earth, 98, 4553-4565,
321 Tichelaar, B. W., and L. J. Ruff (1989). Howgood are our best models? Jackknifing, bootstrapping,
322 and earthquake depth. Eos, Transactions American Geophysical Union, 70(20), 593.
323 Wald, D. J. and P. G. Somerville (1995). Variable-slip rupture model of the great 1923 Kanto, Japan,
324 earthquake: geodetic and body-waveform analysis, Bull. Seism. Soc. Am., 85, 159–177.
325 Weatherall, P., K. M. Marks, M. Jakobsson, T. Schmitt, S. Tani, J. E. Arndt, M. Rovere, D. Chayes, V.
326 Ferrini, R. Wigley (2015). A new digital bathymetric model of the world's oceans. Earth Space Sci
327 2, 331-345.
328 Yamamoto, N., S. Aoi, K. Hirata, W. Suzuki, T. Kunugi, and H. Nakamura, (2016) Multi-index method
329 using offshore ocean-bottom pressure data for real-time tsunami forecast. *Earth Planet Space* **68**,
330 128, https://doi.org/10.1186/s40623-016-0500-7
331 Yamanaka, Y. and Y. Tanioka (2021) Study on the 1906 Colombia-Ecuador Megathrust Earthquake
332 Based on Tsunami Waveforms Observed at Tide Gauges: Release Variation of Accumulated Slip
333 Deficits in the Source Area, J. Geophys. Res.: Solid Earth, 126(5), e2020JB021375.
334 Yamanaka, Y. and Y. Tanioka,(2022) Short-wave run-ups of the 1611 Keicho tsunami along the
335 Sanriku Coast, Prog. Earth Planet. Sci., 9, 37.
336 Yanagisawa, H., and K. Goto (2017) Source model of the 1703 Genroku Kanto earthquake tsunami
337 based on historical documents and numerical simulations: modeling of an offshore fault along the
338 Sagami Trough, Earth, Planets Space, 69:136.

APPENDIX

We computed tsunami waveforms at 4 tide gauge stations without the subfault 4C where a large slip of 9 m was estimated by the joint inversion. The observed tsunami waveforms were compared with both the tsunami waveforms computed using the estimated slips at all subfaults and those computed using the estimated slips without subfault 4C in Figure A1. Variance Reduction (VRO, defined by Chikasada et al., 2016) was calculated for both comparisons. Figure A1 clearly shows that the tsunami generated from subfault 4C affects a later part of the first pulse at 3 tide gauge stations in Tokyo Bay. The variance reduction with tsunami waveforms computed from all subfaults was 86.4%, while that with tsunami waveforms computed from those without subfault 4C decreased to 78.8 %.

1) NTT DATA Corporation, Toyosu Center Building, 3-3-3 Toyosu, Koto City, Tokyo, Japan, 135-0061

2) Institute of the Seismology and Volcanology, Faculty of Science, Hokkaido University, N10W8 Kita-ku Sapporo, Japan, 060-0810

3) Graduate School of Science, Hokkaido University, Sapporo, N10W8 Kita-ku Sapporo, Japan, 060-0810

Corresponding Author: Yuichiro Tanioka e-mail: tanioka@sci.hokudai.ac.jp

Figure Captions

Figure 1. Tectonic setting near the source area of the 1923 Kanto earthquake. a) the source areas of the 1923 Kanto earthquake (orange) and the 1703 Genroku Kanto earthquake (green). Red triangles show location of tide gauges where tsunamis generated by the 1923 Kanto earthquake were observed. b) maximum tsunami surveyed heights (Aida 1993) along the east coast of the Izu Peninsula shown in a red rectangle in (a).

Figure 2. location of 683 survey points observed the coseimic crustal deformation (Namegya et al., 2010). The vertical co-seismic crustal deformation associated with the 1923 Kanto earthquake was revealed by leveling surveys conducted in 1898 and 1923 before and after the earthquake, respectively.

Figure 3. Comparison of topography of Tokyo in the Taisho era when the 1923 earthquake occurred and that of now. (top) current topography was superimposed on Taisho era topography. (bottom) an aerial photograph of recent Tokyo Bay area. Red circles show location of tide gauges where tsunami waveforms were observed.

Figure 4. Locations of subfaults along the plate interface along the Sagami Trough where the Philippine Sea Plate subducts. Blue dashed contours show the depth of the plate interface with a 2 km interval. Red triangles show locations of tide gauges where tsunami waveforms were observed.

Figure 5. Results of the joint inversion of tsunami waveforms and crustal deformation data. a) the estimated slip distribution of the 1923 Kanto earthquake. Red triangles show locations of tide gauges where tsunami waveforms were observed. Two blue dashed ellipsoids, I and II, show large slip areas.

411 A blue star shows the epicenter of the Kanto earthquake. Black contours show the slip distribution
412 estimated by Matsuura et al. (2007) with a contour interval of 2 m. Two blue dashed ellipsoids, I and
413 II, show large slip areas. b) comparison of observed (blue) and computed (orange) tsunami waveforms.
414 Yellow hatched areas show parts of tsunami waveforms used in the joint inversion.
415
416 Figure 6. Comparison of observed and computed vertical crustal deformation caused by the 1923
417 Kanto earthquake. Dark and light blue arrows show observed uplifts and subsidence, respectively. Red
418 and orange arrows show computed uplifts and subsidence, respectively.
419
420 Figure 7. Slip distributions estimated from the joint inversion of tsunami waveforms and crustal
421 deformation data using different weighting factors (λ), the weight of the crustal deformation data
422 against the tsunami data, 0.25, 0.5, 0,75, 1.0, and 2.0. Blue allows show subfault 4C where a large slip
423 was estimated in this study but not in previous studies.
424
425 Figure 8. Comparison of surveyed tsunami heights (red dots), computed maximum tsunami heights
426 from the estimated slip distribution (blue dots), and those from the slip distribution without subfault
427 4C (green dots), along the east coast of the Izu Peninsula. (bottom) maximum tsunami height
428 distribution near the east coast of the Izu peninsula computed from the estimated slip distribution.
429
430 Figure A1. Comparison of observed tsunami waveforms (blue), computed tsunami waveforms from
431 the estimated slip distribution (orange), and those from the slip distribution without subfault 4C (green).
432 The deference between two computed tsunami waveforms, orange and green curves, appears later
433 parts of tsunami waveforms.
434

435

436 Table 1. Parameters of subfault and the estimated slip distribution of the 1923 Kanto Earthquake

subfault name	*longitude (º)	*latitude (º)	shallowest depth (km)	strike for top of subfault (º)	slip amount (m)	error (m)
A1	139.093	35.702	22	291	3.4	1.9
A2	139.053	35.571	18	293	1.1	1.8
A3	139.005	35.414	11	273	8.3	1.6
A4	138.970	35.301	2	288	0.0	3.3
B1	139.297	35.640	22	293	3.8	1.8
B2	139.233	35.511	18	293	6.0	2.3
B2	139.172	35.386	11	295	11.0	2.8
B4	139.112	35.265	2	300	5.3	1.3
C1	139.467	35.581	22	296	0.0	0.0
C2	139.392	35.456	18	294	0.0	0.0
C3	139.317	35.330	10	299	1.9	0.9
C4	139.243	35.205	2	309	9.2	1.4
D1	139.648	35.510	22	292	1.8	0.4
D2	139.570	35.391	18	292	0.0	0.6
D3	139.483	35.256	11	301	3.5	0.5
D4	139.388	35.108	2	318	0.0	0.7
E1	139.814	35.454	22	287	1.1	0.5
E2	139.737	35.335	18	291	4.7	1.0
E3	139.636	35.180	10	302	6.0	0.6
E4	139.516	34.993	2	312	0.0	1.1
F1	139.995	35.408	22	280	0.8	0.3
F2	139.913	35.281	18	286	0.0	0.0
F3	139.795	35.098	10	304	5.9	0.5
F4	139.659	34.887	2	318	3.6	1.7
G1	140.215	35.337	22	268	0.3	0.2
G2	140.117	35.196	17	281	0.4	0.2
G3	140.001	34.982	10	299	0.0	0.1
G4	139.869	34.735	3	309	2.5	1.5

437 *longitude and latitude show the southeast corner of subfaults

438

Figure1

Click here to access/download;Figure;Fig1.jpg

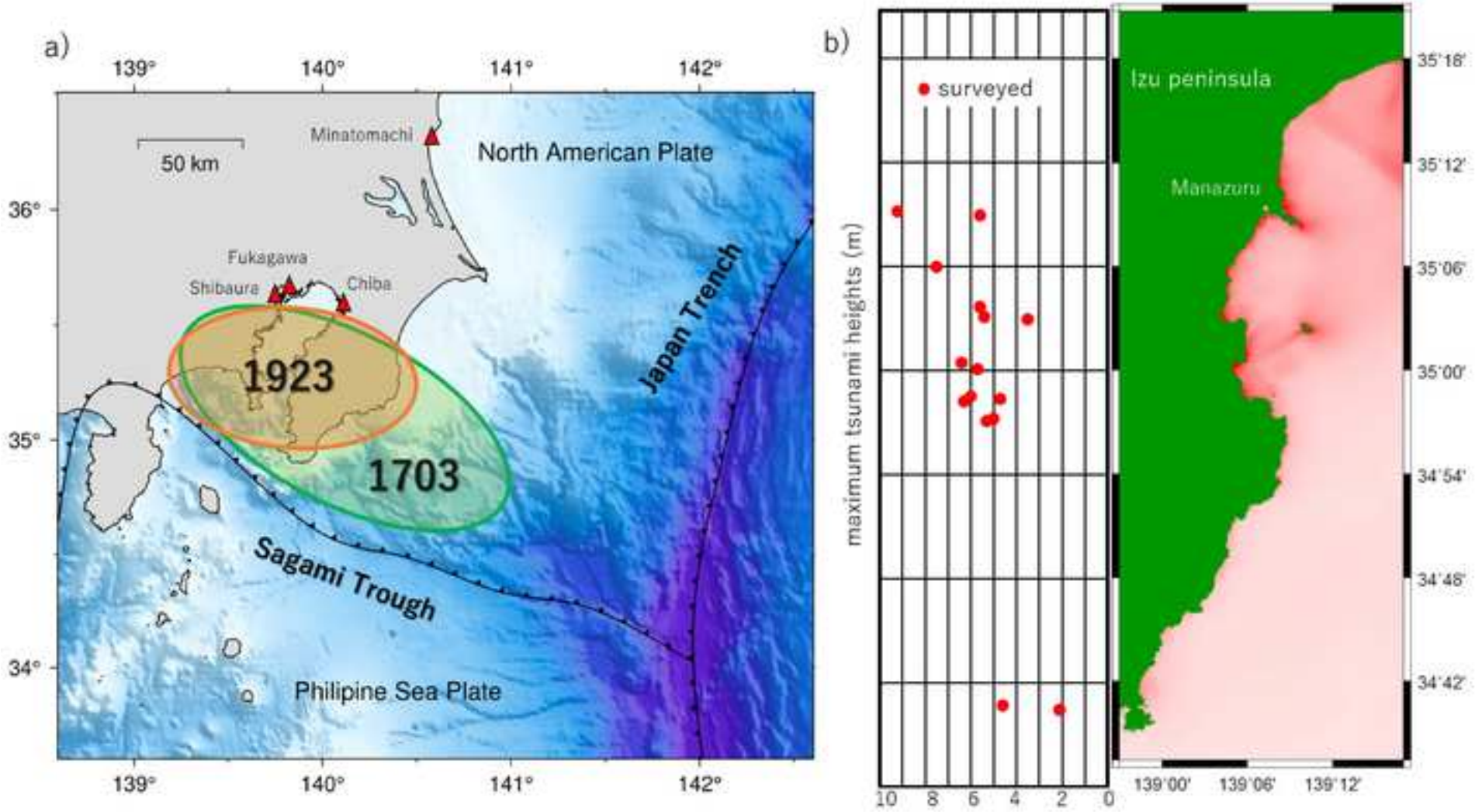


Figure2

Click here to access/download;Figure;Fig2.jpg

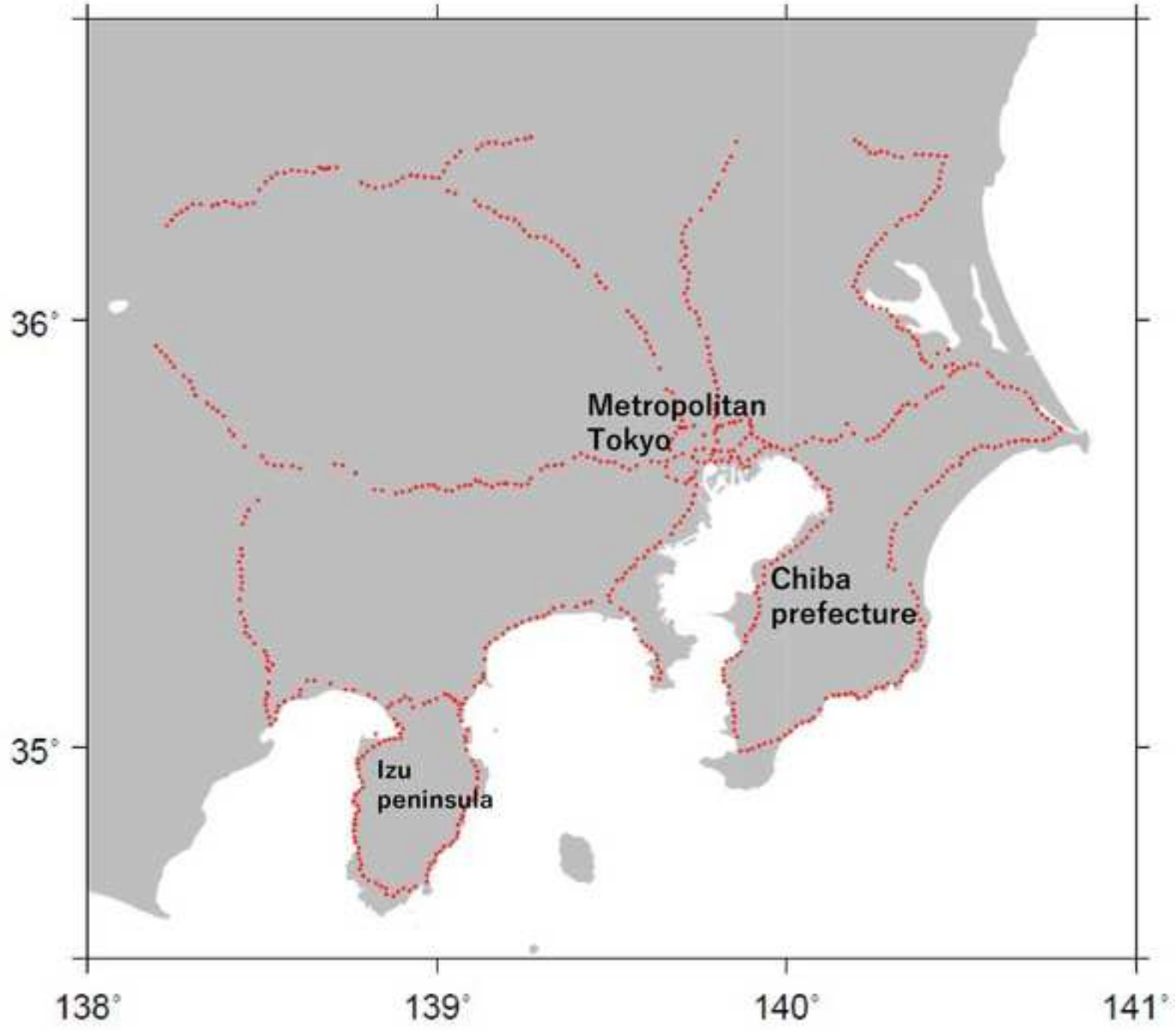


Figure3

Click here to access/download;Figure;Fig3.jpg



Figure4

Click here to access/download;Figure;Fig4.jpg

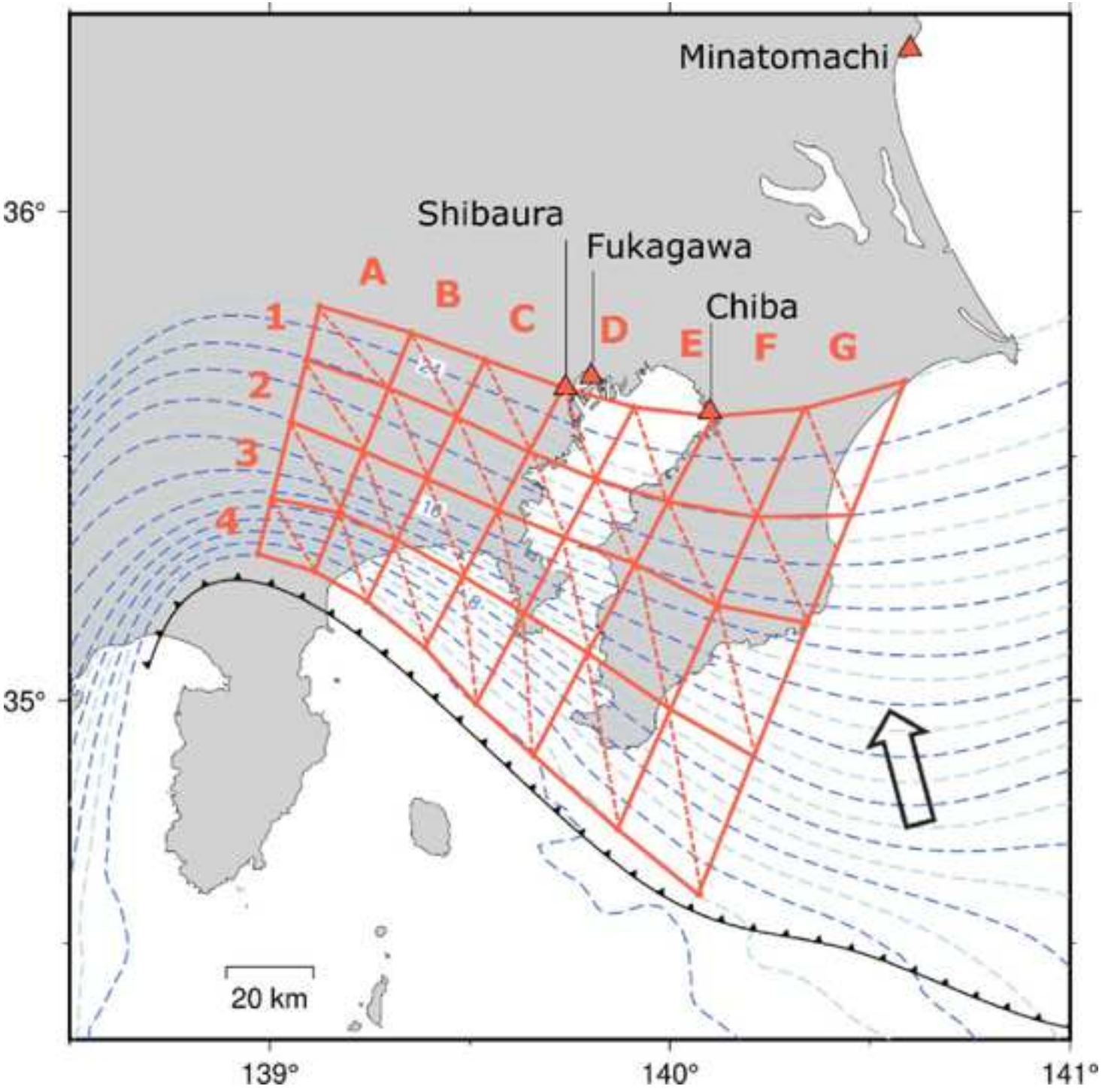


Figure5

Click here to access/download;Figure;Fig5.jpg

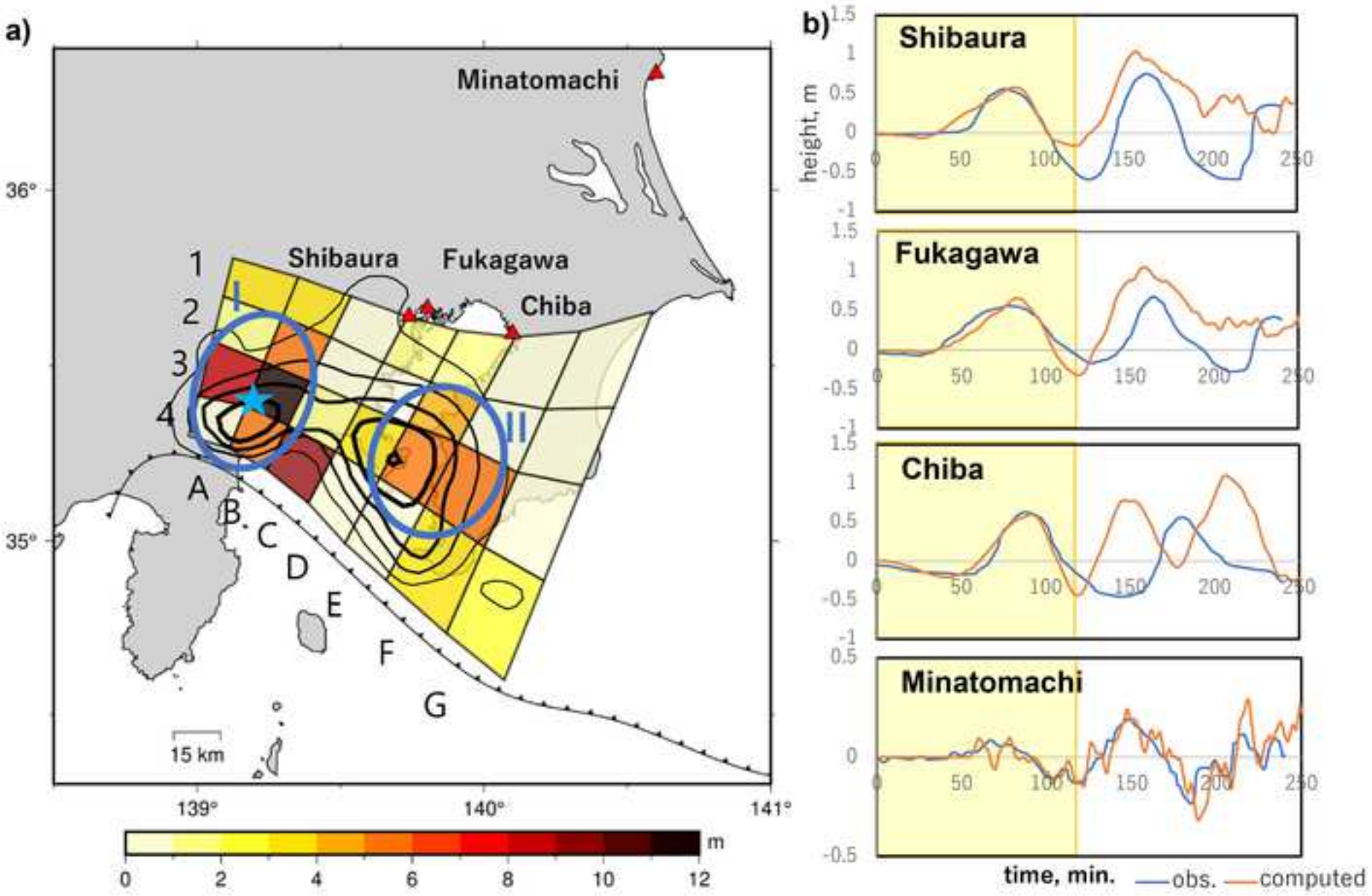


Figure6

Click here to access/download;Figure;Fig6.jpg

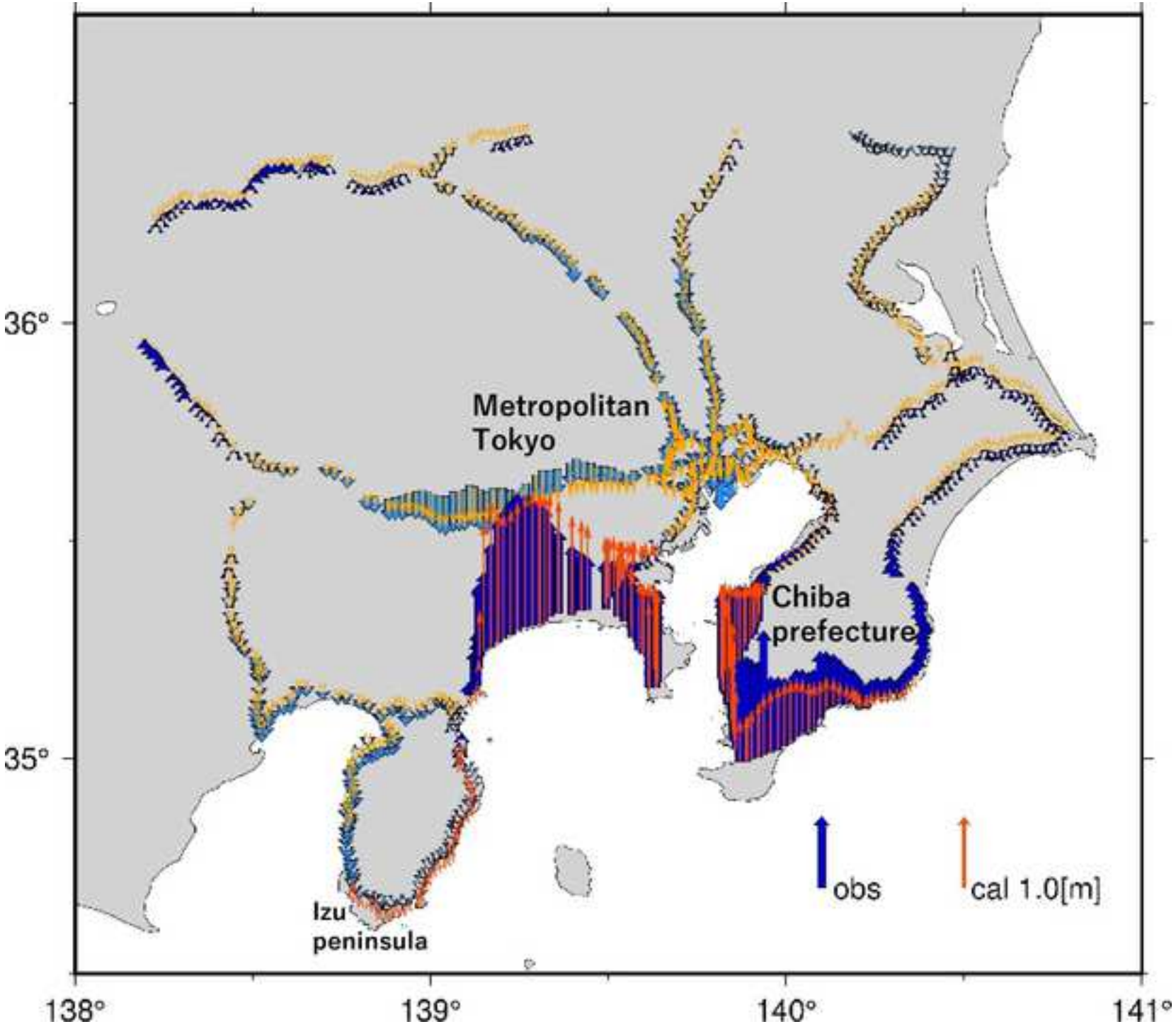
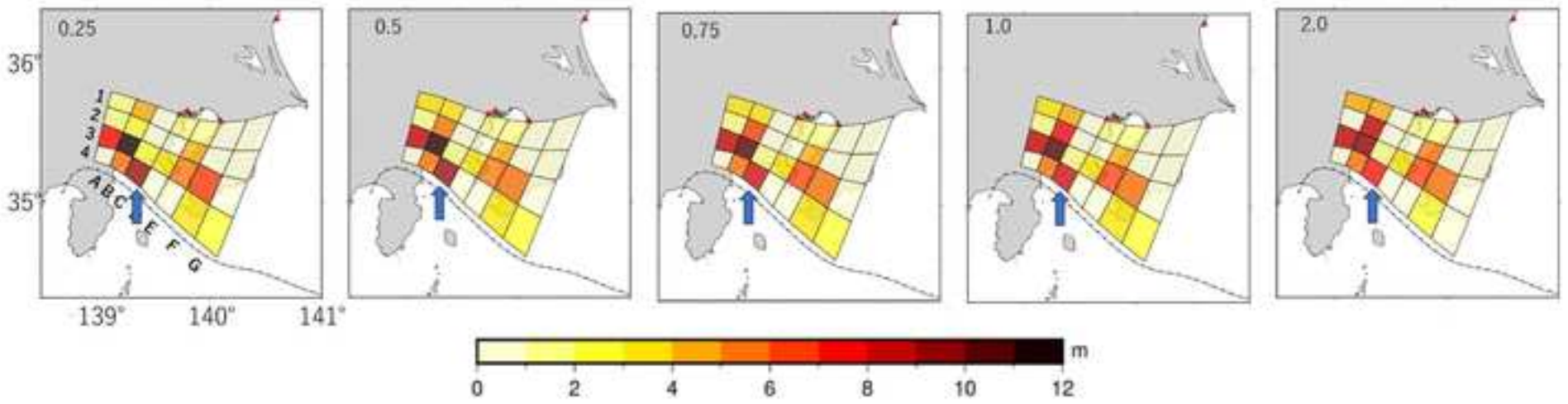


Figure7

Click here to access/download;Figure;Fig7.jpg



Click here to access/download;Figure;Fig8.jpg

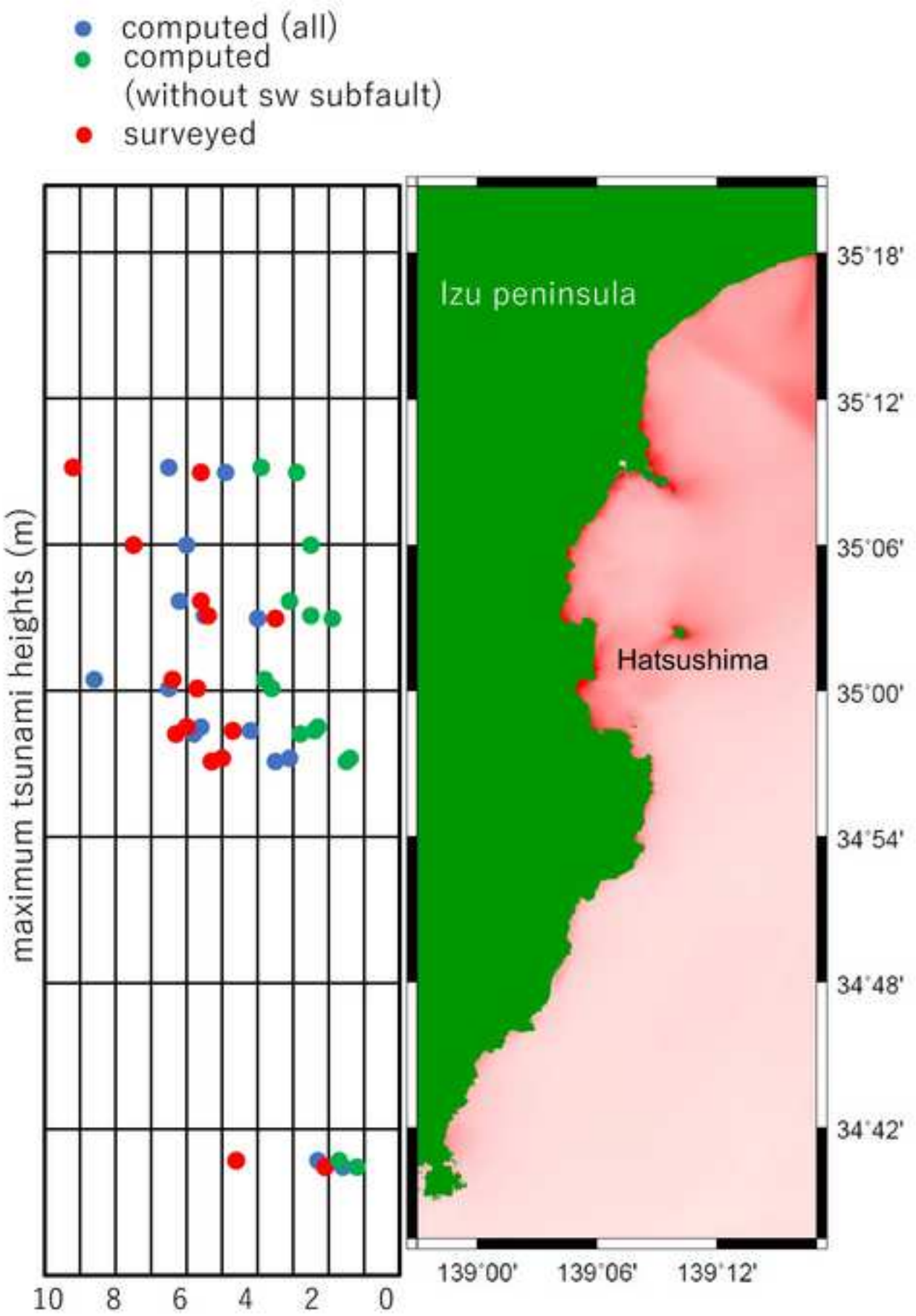
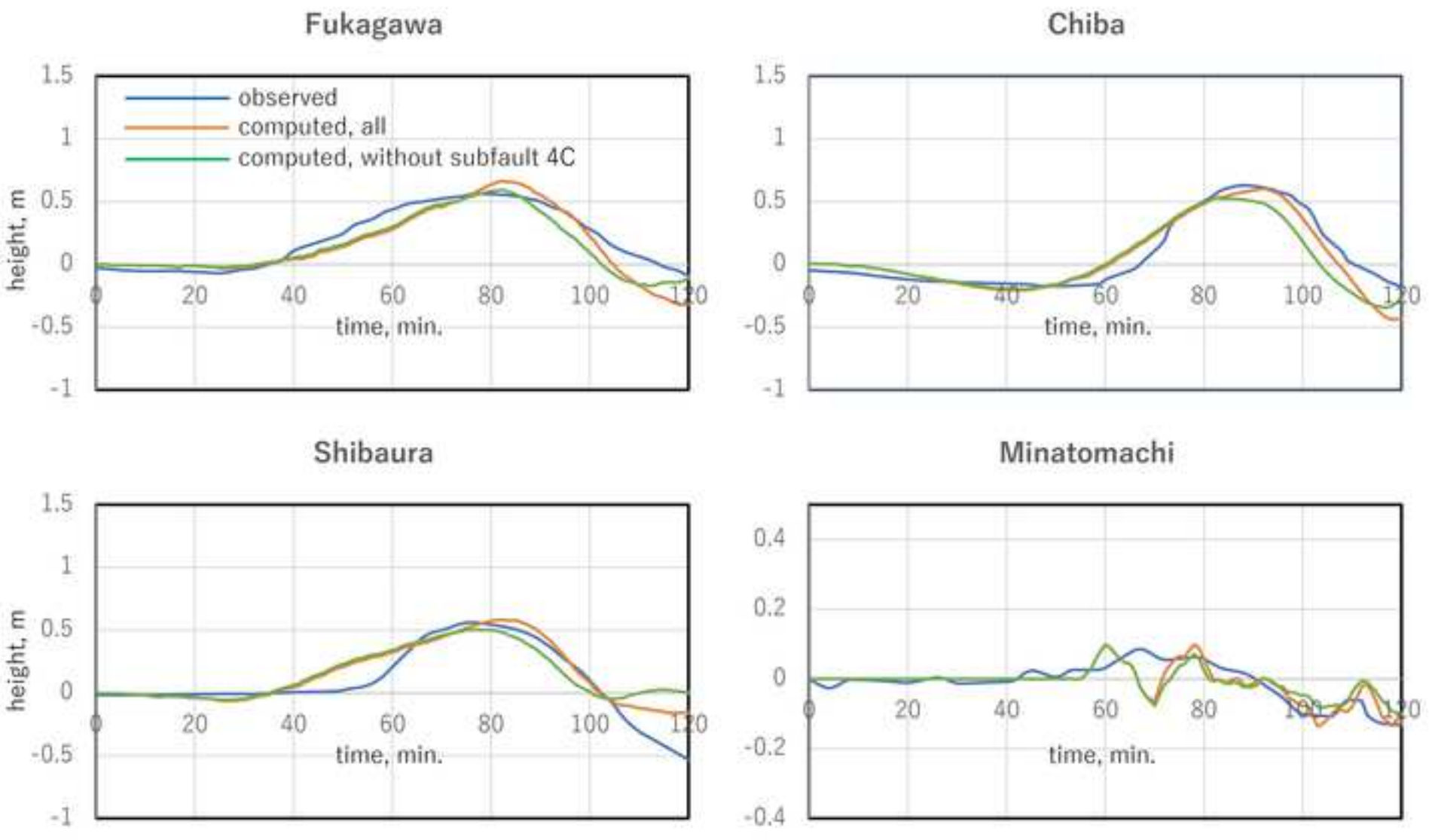


Figure8

FigureA1

Click here to access/download;Figure;FigA1.jpg



Supplemental Material (Main Page, Tables, Figures) Click here to access/download;Supplemental Material (Main Page, Tables, Figures);Supplemental material.docx

Supplemental Material

Re-estimating a source model for the 1923 Kanto earthquake by joint inversion of tsunami waveforms and co-seismic deformation data

Yumi Nakadai[1)], Yuichiro Tanioka[2)], Yusuke Yamanaka[2)], and Tatsuya Nakagaki[3)]

1) NTT DATA Corporation, Toyosu Center Building, 3-3-3 Toyosu, Koto City, Tokyo, Japan, 135-0061
2) Institute of the Seismology and Volcanology, Faculty of Science, Hokkaido University, N10W8 Kita-ku Sapporo, Japan, 060-0810
3) Graduate School of Science, Hokkaido University, Sapporo, N10W8 Kita-ku Sapporo, Japan, 060-0810

Corresponding Author: Yuichiro Tanioka e-mail: tanioka@sci.hokudai.ac.jp

Part 1: Fault parameters of subfaults

The fault parameters of all triangle subfaults faults in Figure 3 are shown in Table S1.

Table S1. Fault parameters of all subfaults. Two triangle faults (a and b) are in each subault.

subfault name	first point			second point			third point			strike (º)	rake (º)
	Longitude (º)	latitude (º)	depth, km	Longitude (º)	latitude (º)	depth, km	longitude (º)	latitude (º)	depth, km		
1A (a)	130.1250	35.8071	25	139.0929	35.7024	22	139.3534	35.7538	25	291	126
1A (b)	139.0929	36.7024	22	139.2975	35.6402	22	139.3534	35.7538	25	287	122
2A (a)	139.0929	36.7024	22	139.0528	35.5715	18	139.2975	35.6402	22	293	128
2A (b)	139.0528	35.5715	18	139.2334	35.5109	18	139.2975	35.6402	22	291	126
3A (a)	139.0528	35.5715	18	139.0049	35.4144	11	139.2334	35.5109	18	273	108
3A (b)	139.0049	35.4144	11	139.1716	35.3858	11	139.2334	35.5109	18	293	128
4A (a)	139.0049	35.4144	11	138.9704	35.3009	2	139.1716	35.3858	11	288	123
4A (b)	138.9704	35.3009	2	139.1121	35.2648	2	139.1716	35.3858	11	276	111
1B (a)	139.3534	35.7528	25	139.2975	35.6402	22	139.5373	35.6982	25	293	128
1B (b)	139.2975	35.6402	22	139.4670	35.5810	22	139.5373	35.6982	25	290	125
2B (a)	139.2975	35.6402	22	139.2334	35.5109	18	139.4670	35.5810	22	293	128
2B (b)	139.2334	35.5109	18	139.3921	35.4556	18	139.4670	35.5810	22	293	128
3B (a)	139.2334	35.5109	18	139.1716	35.3858	11	139.3921	35.4556	18	295	130
3B (b)	139.1716	35.3858	11	139.3174	35.3302	2	139.3921	35.4556	18	293	128
4B (a)	139.1716	35.3858	11	139.1121	35.2638	2	139.3174	35.3302	10	300	135
4B (b)	139.1121	35.2638	2	139.2430	35.2048	2	139.3174	35.3302	10	295	130
1C (a)	139.5373	35.2648	25	139.4670	35.5810	22	139.7336	35.6410	25	296	131
1C (b)	139.4670	35.5810	22	139.6480	35.5099	22	139.7336	35.6410	25	290	125
2C (a)	139.4670	35.5810	22	139.3921	35.4556	18	139.6480	35.5099	22	294	129
2C (b)	139.3921	35.4556	18	139.5704	35.3907	18	139.6480	35.5099	22	296	131
3C (a)	139.3921	35.4556	18	139.3174	35.3302	10	139.5704	35.3907	18	299	134
3C (b)	139.3174	35.3302	10	139.4828	35.2556	10	139.5704	35.3907	18	294	129
4C (a)	139.3174	35.3302	10	139.2430	35.2048	2	139.4828	35.2556	10	309	144
4C (b)	139.2430	35.2048	2	139.3878	35.1084	2	139.4828	35.2556	10	299	134
1D (a)	139.7336	35.6410	25	139.6480	35.5099	22	139.9100	35.6012	25	292	127
1D (b)	139.6480	35.5099	22	139.8141	35.4542	22	139.9100	35.6012	25	285	120
2D (a)	139.6480	35.5099	22	139.5704	35.3907	18	139.8141	35.4542	22	292	127

2D (b)	139.5704	35.3907	18	139.5156	35.9931	18	139.8141	35.4542	22	292	127
3D (a)	139.5704	35.3907	18	139.4828	35.2556	10	139.5156	35.9931	18	301	136
3D (b)	139.5156	35.9931	10	139.6362	35.1800	10	139.5156	35.9931	18	292	127
4D (a)	139.5156	35.9931	10	139.3878	35.1084	2	139.6362	35.1800	10	318	153
4D (b)	139.3878	35.1084	2	139.5158	34.9931	2	139.6362	35.1800	10	301	136
1E (a)	139.9100	35.6012	25	139.8141	35.4542	22	140.1093	35.5828	25	287	122
1E (b)	139.8141	35.4542	22	139.9953	35.4080	22	140.1093	35.5828	25	276	111
2E (a)	139.8141	35.4542	22	139.7366	35.3350	18	139.9953	35.4080	22	291	126
2E (b)	139.7366	35.3350	18	139.9128	35.2809	18	139.9953	35.4080	22	287	122
3E (a)	139.7366	35.3350	18	139.6362	35.1800	10	139.9128	35.2809	18	302	137
3E (b)	139.6362	35.1800	10	139.7945	35.0980	10	139.9128	35.2809	18	291	126
4E (a)	139.6362	35.1800	10	139.5158	34.9931	2	139.7945	35.0980	10	312	147
4E (b)	139.5158	34.9931	2	139.6589	34.8871	2	139.7945	35.0980	10	302	137
1F (a)	140.1093	35.5828	25	139.9953	35.4080	22	140.3361	35.5986	25	280	115
1F (b)	139.9953	35.4080	22	140.2150	35.3767	22	140.3361	35.5986	25	265	100
2F (a)	139.9953	35.4080	22	139.9128	35.2809	18	140.2150	35.3767	22	286	121
2F (b)	139.9128	35.2809	18	140.1168	35.1958	17	140.2150	35.3767	22	280	115
3F (a)	139.9128	35.2809	18	139.7945	35.0980	10	140.1168	35.1958	17	304	139
3F (b)	139.7945	35.0980	10	140.0013	34.7350	10	140.1168	35.1958	17	287	122
4F (a)	139.7945	35.0980	10	139.6589	34.8871	2	140.0013	34.7350	10	318	153
4F (b)	139.6589	34.8871	2	139.8688	34.7350	2	140.0013	34.7350	10	304	139
1G (a)	140.3361	35.5986	25	140.2150	35.3767	22	140.5877	35.6544	25	268	104
1G (b)	140.2150	35.3767	22	140.4522	35.3808	22	140.5877	35.6544	25	254	89
2G (a)	140.2150	35.3767	22	140.1168	35.1958	17	140.4522	35.3808	22	281	116
2G (b)	140.1168	35.1958	17	140.3430	35.1589	17	140.4522	35.3808	22	268	103
3G (a)	140.1168	35.1958	17	140.0013	34.9819	10	140.3430	35.1589	17	299	134
3G (b)	140.0013	34.9819	10	140.2091	34.8850	10	140.3430	35.1589	17	281	116
4G (a)	140.0013	34.9819	10	139.8688	34.7350	2	140.2091	34.8850	10	309	143
4G (b)	139.8688	34.7350	2	140.0709	34.6002	2	140.2091	34.8850	10	299	134

Part 2: Summary of the 1923 Kanto earthquake in Aida (1993)

Aida (1993) estimated source models of historical large earthquakes occurred along the Sagami Trough. A description of the 1923 Kanto earthquake by Aida (1993) is summarized here. The best source model which could explain the tsunami height distribution (Table S2) was determined from 7 different source models. The best model was shown in blue rectangles in Figure S1, which include two sources in the subduction zone and one fault off the Izu peninsula. Aida (1993) concluded that one fault off the Izu peninsula is necessary to explain the tsunami height distribution in the Izu peninsula. The surveyed tsunami heights along the Izu peninsula (Aida, 1993) were compared with the maximum tsunami heights computed from the estimated slip distribution and from that without subfault 4C in Table S2.

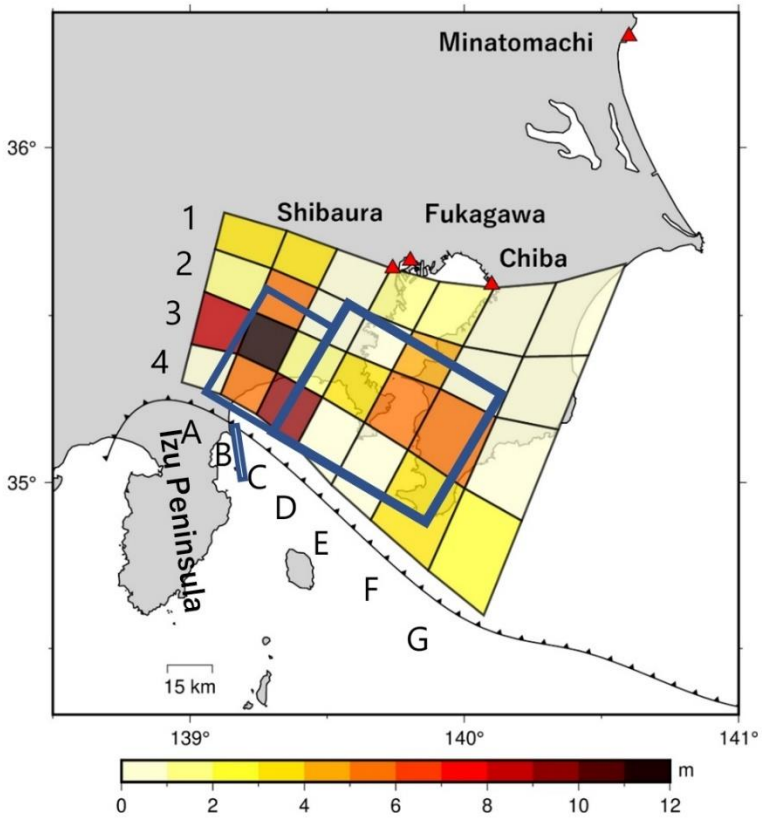


Figure S1 The best fault model of the Kanto earthquake by Aida (1993), three blue rectangles. The slip distribution estimated in this study is also shown by colored quadrilaterals.

Table S2 The surveyed tsunami heights in Izu Peninsula (Aida, 1993) and two computed maximum tsunami heights using the slip distribution on all subfaults and that without subfault 4C.

Location Name	surveyed height, (m)	computed maximum height, (m)		location, (º)	
		all subfaults	without 4C	Longitude	latitude
Manazuru	8.6-9.2	6.5	3.9	139.142	35.153
Fukuura	5.6	4.9	2.9	139.163	35.150
Atami	7.0-7.5	6.0	2.5	139.077	35.100
Kamitaga	4.8-6.4	6.2	3.1	139.073	35.061
Shimotaga	5.4	5.5	2.5	139.070	35.051
Amishiro	3.5	4.0	1.9	139.072	35.049
Usami (Tomata)	6.4	8.6	3.8	139.086	35.008
Usami (Hazu)	3.9-5.7	6.5	2.3	139.083	35.002
Ito (Matsubara)	6.0	5.6	2.3	139.096	34.975
Ito (Ookawa)	3.7-4.7	4.2	2.4	139.098	34.973
Ito (Minato)	6.3	5.8	2.8	139.104	34.971
Kawana (Minato)	5.3	3.5	1.5	139.132	34.952
Kawana (Syuraku)	5.0	3.1	1,4	139.137	34.954
Shimoda (Kakizaki)	4.6	2.3	1,7	138.973	34.678
Shimoda	2.1	1.6	1.2	138.947	34.674